Synthesis, Crystals structures and theoretical studies of novel alkali copper indium orthophosphates $ACuIn(PO_4)_2$ (A = Na, K and Rb).

Abdessalem Badri,[a*] Sami Slimi,[b] Ines Mokni,[a] Necmi Dege,[c] Rosa Maria Solé,[b] Magdalena Aguiló,[b] Francesc Díaz,[b] Xavier Mateos,[b,d] and Mongi Ben Amara [a]

[a]*Laboratory of Interfacial and Advanced Materials, Faculty of Sciences, University of Monastir, 5000 Monastir, Tunisia*
[b]*Universitat Rovira i Virgili (URV), Física i Cristal·lografia de Materials (FiCMA), Marcel·lí Domingo, 1, 43007 Tarragona, Spain*
[c]*Ondokuz Mayıs University, Faculty of Arts and Sciences, Department of Physics, 55139, Kurupelit, Samsun, Turkey*
[d]*Serra Húnter Fellow*
***Corresponding author:** badri_abdessalem@yahoo.fr

Abstract:

$ACuIn(PO_4)_2$ compounds (A=K and Rb) have been prepared by the flux method and solid-state reaction. They were characterized by X-ray diffraction (XRD), Scanning Electron Microscopy (SEM) with Energy Dispersive X-Ray analysis (EDX), Fourier Transform Infra-Red (FTIR), Raman and optical spectroscopies, as well as a Density Functional Theory (DFT) study has been performed. Single XRD analysis shows that the compounds were isostructural and crystallize in the monoclinic centrosymmetric $P2_1/n$ space group. There are one A (Na, K or Rb), one Cu, one In, two P and eight O sites in the asymmetric unit of the $ACuIn(PO_4)_2$ structure. Its structure is made up from corners-sharing between InO_6 octahedra and Cu_2O_8 units, built up from edge-sharing of two CuO_5 polyhedra, to form zigzag chains ranging infinitely along the **b** axis. The inter-connection between these chains is assured by the PO_4 tetrahedra creating a 3D framework with six-sided tunnels parallel to the [101] direction, where the A^+ ions are located. XRD diagrams of the powder samples reveal the formation of single phases with monoclinic symmetry. FTIR and Raman spectroscopies revealed the presence of two isolated PO_4 groups in the analyzed phosphates. The SEM-EDX verifies the morphology and the chemical composition of the synthesized samples. The diffuse reflectance spectroscopy (DRS) has proven an indirect bandgap of 3.34 eV, 3.33 and 2.82 eV for $NaCuIn(PO_4)_2$, $KCuIn(PO_4)_2$ and $RbCuIn(PO_4)_2$, respectively. The electronic bandgap structure and bonding character analysis of important atom pairs in the $ACuIn(PO_4)_2$ structure are also studied in detail.

Keywords: Indium phosphates; Flux method; Single crystal; EDX; optical properties.

1. Introduction

Inorganic phosphates are a class of materials that have aroused considerable interest in the latest decades. They offer structural flexibility resulting from the way in which the PO_4^{3-} phosphate groups are assembled with the oxygenated polyhedra of the metal and/or rare-earth ions (M, Ln) to generate a stable phosphate material. Indeed, different crystalline structures have been produced, a two-dimensional lattice (2D) or a three-dimensional network (3D) with hexagonal, rectangular or triangular tunnels containing the alkali cations. These structural assemblies can be entirely tetrahedral (PO_4/MO_4) or made of multiple types of polyhedra (PO_4/ MO_4, MO_5 or MO_6). The physico-chemical properties of monophosphates are directly correlated with the nature and oxidation degree of the metal cations introduced into the structure, regardless openning degree. Alkaline monophosphates with structure-type Nasicon [1], Alluaudite [2] and Olivine [3] were widely studied for their important electrochemical properties [4, 5]. They are used as electrodes for lithium and sodium batteries [6, 7, 8, 9]. Similarly, they are considered as non-linear optical materials [10, 11], sensors for NO_x detection in the atmospheric environment [12], etc. While the study of metal phosphates is apparent and many inspiring results have recently been obtained, there is very little work in the literature addressing alkali metal phosphates including indium atoms. Recently, alkali phosphates with indium have been studied, as examples $Na_{2.22}Mn_{0.87}In_{1.68}(PO_4)_3$ [13], $Na_{1.85}Mg_{1.85}In_{1.15}(PO_4)_3$ [14] and $NaMn(Fe_{1-x}In_x)_2(PO_4)_3$, $(Na_{1-x}Li_x)CdIn_2(PO_4)_3$ solid solutions [15, 16]. These are isotypic and exhibit Alluaudite-type structures. Besides, as for the double indium phosphates $A_3In(PO_4)_2$, only the β and α allotropic varieties of the compound $Na_3In(PO_4)_2$ are known [17, 18]. The low-temperature β-form of $Na_3In(PO_4)_2$ resembles the Rcanite-type phosphates $K_3Y(PO_4)_2$. The same is also true for the β-$Na_3M^{III}(PO_4)_2$ compounds (where M^{III} = La–Lu), whose structure is characterized by an assortment of β-K_2SO_4 and Na_2CrO_4 structural motifs [19]. $K_3In(PO_4)_2$ and $Rb_3In(PO_4)_2$ [20] have shown analogous network topology, which are respectively built by structural units $[In(PO_4)_2]$ and $[In_2(PO_4)_4]$.

In our extensive research of the ternary system A_3PO_4-$M_{3/2}PO_4$-MPO_4, we turned to the synthesis of two new compounds, the $ACuIn(PO_4)_2$ (A=K, Rb) that complement the series together with $NaCuIn(PO_4)_2$ which was synthesized as single crystal [21]. We report in this work their crystal structures determined by XRD as well as their characterization by SEM-EDXand FTIRand Raman spectroscopies. We show a detailed description of their electronic properties obtained through DFT theoretical studies.

2. Experimental

2.1. Synthesis of the crystals

Single crystals with chemical formula $ACuIn(PO_4)_2$ (A=K and Rb) were grown in a flux of alkali dimolybdate $A_2Mo_2O_7$ corresponding to a molar ratio of P:Mo=2:1. A mixture of KNO_3 (Fluka, 99%, 20 mmol), Rb_2CO_3 (Acros, 99%, 10 mmol), $Cu(NO_3)_2{\cdot}6H_2O$ (Fluka, 99%, 10 mmol), In_2O_3 (Acros, 99%, 5 mmol),$(NH_4)_2HPO_4$ (Merck, 99%,20 mmol) and MoO_3 ((Acros, 99%, 10 mmol) were dissolved in a nitric acid/distilled water solution. The resulting mixture was evaporated by heating at 353 K for 24 h. The resulting dry residue was ground in an agate mortar, placed in a platinum crucible and subsequently heated in open air for 24 h at 673 K to expel the decomposition products CO_2, NH_3 and H_2O. The sample was then reground and melted for 1 h at 1173 K. The cooling process consisted of two steps, firstly slow cooling to 673 K at a rate of 10 $°Ch^{-1}$, and secondly, quick cooling toroom temperature. Finally, the crystals were extracted by washing the mixture with boiling water to dissolve the residual flux. They consisted of green crystals with hexagonal morphology.

Besides, the polycrystalline samples were synthesized by solid-state reaction method, starting from a stoichiometric mixture of the raw materials in the following molar ratio: A:Cu:In:P=1:1:1:2. The raw materials ANO_3 (A=Na, K), Rb_2CO_3, $Cu(NO_3)_2.6H_2O$, In_2O_3 and $(NH_4)_2HPO_4$ were dissolved in a nitric acid solution. After a primary treatment, analogous to that assumed for the synthesis of the single crystals until 873 K, the sample was subjected to final calcination at 1053 K for 48 h with intervening grinding. A green powder was obtained by thermal quenching in air.

2.2. Characterization techniques

Single crystals with dimensions 0.28×0.32×0.42 mm and 0.34×0.56×0.67 mm of $KCuIn(PO_4)_2$ and $RbCuIn(PO_4)_2$, respectively, were selected for the structure determination. The X-ray data were collected at room temperature with a STOE IPDS-II diffractometer using graphite monochromated MoK_α radiation (λ = 0,71073 Å) operating with a maximum 2θ value of 50.00° in a series of ω scans in 1° oscillations and then integrated using the Stoe X-AREA [22] software package. The analysis of the systematic absences led to the assignment of the centrosymmetric monoclinic space group $P2_1/n$. The data were then corrected for Lorentz and Polarization effects and the numerical absorption correction was performed using the X-RED [23] and X-SHAPE [24] softwares.

Crystal symmetry and purity of the synthesized polycrystalline samples were assessed using a Philips X'Pert automatic diffractometer with Ni-filtered Cu-Kα radiation (λ = 1.5406

Å). Chemical composition and morphology analysis were evaluated by a scanning electron microscope (SEM, S-4800, Hitachi) coupled to an energy dispersive X-ray spectrometer (EDX). Infrared (IR) spectra were recorded in the range from 400 to 1800 cm^{-1} using a Perkin Elmer Paragon 1000 PC Fourier spectrometer. Raman spectra were obtained using a Renishaw inVia micro-Raman confocal microscope, the λ_{exc} was 514 nm (Ar^+ ion laser), the spectral resolution was ~1 cm^{-1}. UV-visible diffuse reflectance spectra from 200 to 2000 nm were measured at room temperature considering $BaSO_4$ powder as reference (100% reflectance) and using a Perkin Elmer Lamda-950 UV/VIS/NIR spectrophotometer.

The calculation of the energy band structure and the determination of optical characteristics were considered using the crystallographic data of $ACuIn(PO_4)_2$ (A = K, Rb, Na) obtained by X-ray single crystal diffraction. No further optimization of the geometry was considered during these theoretical studies. The calculations are based on the total energy code CASTEP [27, 28] which uses pseudo-potentials to describe the electron-ion interactions and allows the representation of the electronic wave functions using a set of plane wave bases. The total energy was calculated in the framework of the generalized Perdew-Burke-Ernzerhof gradient approximation (GGA-PBE) [29]. In addition, norm-preserving pseudopotentials [30] were applied for Na, K, Rb, Cu, In, P and O, respectively. The total energy and force convergence thresholds were 1.10^{-6} eV per atom and 0.05 $eV.Å^{-1}$, respectively. The meshes of the k-point set to define the number of integration points that were used to integrate the wave function in the reciprocal space (Figure S1) were 3×2×2 to calculate the bond structure, the density of states and the optical properties for each of the three crystals. The rest of the parameters involved in the calculations were set by the default values of the CASTEP code.

3. Results and discussions

3.1. Structural characterization

The structures were solved by direct methods [25], which revealed one site for the indium atoms and one for the alkali atoms (Rb or K) as well as copper. Successive differences Fourier maps and then refined on F^2 by a full-matrix least-squares [26] led to two distinct positions for the phosphorus atoms and five for the oxygen ones. A final anisotropic refinement of all the atoms converged at R_1= 0.023 and wR_2= 0.052 for $KCuIn(PO_4)_2$, and R_1= 0.059 and wR_2= 0.145 for $RbCuIn(PO_4)_2$ for the observed reflections. The main crystal data and experimental conditions for the intensity measurements and refinements are given in Table 1. Atomic coordinates and equivalent thermal displacements are listed in Table S1 and S2.

Relevant interatomic distances and connection angles for the two $ACuIn(PO_4)_2$ compounds (A = K, Rb) are listed in Table S3.

Further details of the crystalline structural investigation may be obtained from the Fachinformationszentrum Karlsruhe, D-76344 Eggenstein-Leopoldshafen, (Germany), on quoting the depository numbers CSD-2075272 and CSD-2075484 for $KCuIn(PO_4)_2$ and $RbCuIn(PO_4)_2$, respectively.

The crystal data for $KCuIn(PO_4)_2$ and $RbCuIn(PO_4)_2$ evidence their tridimensional structure. The unit cell of $ACuIn(PO_4)_2$ is built on the basis of an asymmetric unit containing A (Na, K or Rb), Cu, In, two P positions and eight oxygen positions (Figure S2). The structural units are Cu_2O_8 dimers of edge-sharing CuO_5 triangular bipyramids, two InO_6 octahedra and four PO_4 tetrahedra. The Cu_2O_8 units share opposite edges with two $P(1)O_4$ tetrahedra and two alternate corners with $P(1)O_4$ and $P(2)O_4$. Accordingly, it can be described using the general formulation $[CuIn(PO_4)_2]^-$. In the structure, these structural units are associated according to the three dimensions of the network (Figure S3) leading to zigzag chains parallel to the **ab** plane. The projection of the structure in the plane (101) shows hexagonal tunnels evolving in the [001] direction, which are occupied by the alkali cations (Figure S4).

The Bond-Valence Sum (BVS) and charge-distribution (CHARDI) calculations were performed using the Chardi-2015 program [31] based on a thorough study of the crystal data obtained from the structural analysis. The obtained results are summarized in Tables S4 and S5. The valences of the cations and anions confirm the electrical neutrality of the synthesized compounds, likewise the effective coordination agrees with the coordination of the cations.

In both compounds, the InO_6 octahedra are slightly distorted, with the two In-O distances ranging from 2.088(3) to 2.250(2) Å and 2.091(4) to 2.251(3) respectively. The average <In-O> distances were determined to be 2.144(1) Å and 2.148(3) which are coherent with the observed values of 2.141(2) and 2.151(2) Å, respectively in $NaCuIn(PO_4)_2$ [21] and $Na_3In_2(PO_4)_3$ [32]. The CuO_5 polyhedra are also distorted with a wide dispersion of the the two Cu-O distances ranging from 1.922(3) to 2.188(3) Å and 1.917(4) to 2.203(4) Å around their mean values <Cu-O> = 2.023(3) Å and 2.026(4) Å. This obvious distortion for Cu^{2+} ($3d^9$) is well known. In an octahedral environment the Cu^{2+} ion deforms its site to stabilize the energy levels of its electrons. This consequence is known as the Jahn-Teller effect [33, 34]. The average distances <P-O> in the two types of $P(1)O_4$ and $P(2)O_4$ tetrahedra are 1.545(3) Å, 1.536(3) Å and 1.546(4) Å, 1.535(4) Å, respectively and are typical in monophosphates [35]. The oxygen environments of the alkali cation (A) located in the large tunnels of the structure were determined using the procedure of Donnay and Allman [36]. Accordingly, the environment of

A consists of nine oxygens. The result AO_9 polyhedra share vertices to form zigzag chains parallel to the [101] direction (Figure S5).

A previous comparative structural study showed that the oxygenate coordination of Cu^{2+} were 5 or 6. $ACuAl(PO_4)_2$ compounds with (A=K, Rb) [37, 38] and $KCuGa(PO_4)_2$ [39] crystallize in *P2₁/c* space group and adopt a standard structure determined by the family of phosphates $AM^{II}M^{III}(PO_4)_2$, obtained by the flux method and under hydrothermal conditions. The crystal structure (Figure 1 (a)) is built from the 3D framework with large tunnels parallel to the **a** axis. The structural framework could be described as an arrangement of five centrosymmetric ribbons $[M^{III}{}_2P_6O_{26}]$ interconnected by top-sharing with the PO_4 tetrahedra (Figure 1 (b)). The CuO_6 octahedra are combined by a common edge-sharing to form zigzag chains (Figure 1 (c)). Potassium, K^+ cations are retained in hexagonal tunnels. The analysis of the structural data of the $ACuM^{III}(PO_4)_2$ family of compounds with M^{III}= Al^{3+}, Ga^{3+} and Cr^{3+} and Fe^{3+}, summarized in Table 2, reveals that the oxygenated environment of Cu^{2+} depends on the steric and chemical factor of the trivalent metal. Therefore, the oxygenated environment of Cu^{2+} varies from 6 to 5 when the ionic radius of the trivalent metal increases and when the metallic character increases which also leads to an octahedral symmetry of the M^{3+}.

The crystal structure characterization of the synthesized sample was performed by applying the Rietveld whole profile fitting method using the FullPROF software [43]. The sample refinement diagrams are shown in Figure S6.

The refinement procedure started by refining the scale factor, the detector zero point, the background parameters and the lattice parameters. Then gradually other parameters were added, such as the peak profile parameters (pseudo-Voigt), the atomic coordinates and the B isotropic displacement parameters. The refinement of the structures was stable at all steps and converged rapidly to the results summarized in Table S6. Further, we observed that the $RbCuIn(PO_4)_2$ pattern showed the presence of a negligible amount (~3%) of raw In_2O_3 phase [44], identified from the xpert High Score plus [45]. Tables S7-S9 reported the atomic coordinates obtained from the Rietveld refinements. The conventional *R* factors of the refinements confirmed that the synthesized powder samples exhibit the same monoclinic symmetry as determined on a single-crystal XRD analysis for the three mentioned compounds.

3.2. Chemical composition

The SEM-EDX was investigated to point out the morphology and to identify the chemical composition of the synthesized materials. The chemical composition of the$NaCuIn(PO_4)_2$ sample was determined from powder.. However, the composition of $KCuIn(PO_4)_2$ and $RbCuIn(PO_4)_2$ were determined from the single crystal (Figure S7(a) and

(b)). Their characterization confirmed the presence of all the chemical elements expected from the chemical formula.

SEM-EDX and EDS of the $NaCuIn(PO_4)_2$ sample are presented in Figure 2. For $NaCuIn(PO_4)_2$, the surface morphology was characterized by an agglomeration of spherical and platelet-like particles. The EDS elemental mapping was used to show the spatial distribution of the elements in a sample and to measure even the elemental distribution in a textural context, and especially for showing compositional zonation. As a result, the EDS attested that all the elements mentioned above are uniformly distributed in the studied surface of the powder sample.

Therefore, the atomic percentages of the different elements of the examined materials grouped in Table S10 agree with their composition.

3.3. Vibrational properties

An isolated PO_4 tetrahedron presents a T_d symmetry. It owns four fundamental modes of vibration. These modes are defined and observed at the following wavenumbers. Symmetric: P-O stretching vibrations ν_1 (A_1) 938 cm^{-1}, O-P-O angle bending vibrations ν_2 (E) 420 cm^{-1}, and antisymmetric: P-O stretching vibrations ν_3 (F_2) 1017 cm^{-1} and O-P-O angle bending vibrations ν_4 (F_2) 567 cm^{-1}. All modes are Raman active, the ν_3 and ν_4 modes are only active in the IR [46,47]. The FTIR spectra of the $ACuIn(PO_4)_2$ (A = Na, K, Rb) samples (Figure 3 (a)) depict the characteristic stretching and bending modes of free PO_4 groups. Indeed, the observed bands at 1220-1038 cm^{-1} were assigned to the antisymmetric stretching modes (ν_3), and the bands detected in the 931-916 cm^{-1} region are assigned to the symmetric stretching modes (ν_1) of the isolated PO_4 tetrahedra. The bands located at 690-545 and 446-410 cm^{-1} were attributed to the asymmetric deformation (ν_4) and symmetric bending (ν_2) of the PO_4 groups, respectively. Finally, the band observed at 638 cm^{-1} was attributed to the presence of In-O and Cu-O modes. The Raman spectra of $ACuIn(PO_4)_2$ (A = Na, K, Rb) are shown in figure 3 (b). The assignment of the different modes were made by comparison to previous works reported on similar monophosphates [48, 49, 50]. Two distinct regions were defined: (1) the bands above 350 cm^{-1} corresponding to the internal modes of PO_4, while (2) the bands below 350 cm^{-1} were ascribed to the external modes of the lattice. The bands observed in the 996-954 and 1108-1008 cm^{-1} regions were attributed to the symmetric (ν_1) and asymmetric (ν_3) stretching modes of the isolated PO_4 groups. The band located at 540 cm^{-1} was assigned to the asymmetric (ν_4) bending mode and those detected in the 457-425 cm^{-1} region to the symmetric (ν_2) bending modes of PO_4 groups. In the analyzed compounds, the vibration modes of the diphosphates groups were not detected. The bands at 353-335 and 279-274 cm^{-1} were correlated to vibrations and translations of In^{3+} ions.

3.4. Theoretical studies of $ACuIn(PO_4)_2$ (A = Na, K, Rb)

3.4.1. Bandgaps and electronic structure

The calculated band structures of $ACuIn(PO_4)_2$ (A = K, Rb, Na) along high-symmetry points of the first Brillouin zone are shown in Figure S8. It can be seen that the top of the is almost flat and close to the Fermi level (0.0 eV), and the bottom of the conduction bands (CB) show the same dispersion for all compounds. The band gaps calculated using GGA for $ACuIn(PO_4)_2$ (A = K, Rb, Na) are 2.315, 2.319 and 2.095 eV, respectively. The VB maximum and the CB minimum are located at various points of the Brillouin zone: G and D. Hence, the three compounds are indirect band gap semiconductor materials. The total density of states of $ACuIn(PO_4)_2$ is given in Figure S9. Te relative energy gaps correspond well to the electronic bands of the band structure which gave the same energy gaps for each crystal.

The reflectance spectra of $ACuIn(PO_4)_2$ shown in Figure 4.(a) were measured under the same experimental conditions in the 200-800 nm wavelength range. The crystals show remarkable absorption in the near infrared region.

Equation (1) was used to identify the correlation between the absorption coefficient of the semiconductor materials and the optical band gap E_g [51]:

$$(\alpha_{abs}.h\nu_{ph})^n = A\left(h\nu_{ph}.E_g\right) \quad (1)$$

Where h is the Plank's constant, ν_{ph} is the photon energy, n is determined by the transition type (n = 1/2, 2, 3/2 or 3 for allowed direct, allowed indirect, forbidden direct and forbidden indirect electronic transitions, respectively). The optical bandgap E_g can be determined from the Tauc plot shown in Figure 4.(b). From the Tauc plot, the optical band gap E_g is determined. The calculated optical band gap for $ACuIn(PO_4)_2$ crystals is slightly higher than those determined from the DFT calculations. This underestimation of the band gaps in regular DFT calculations with GGA comes from the discontinuity of the exchange-correlation energy function [52].

The spectral dependences of the partial electron densities of states for atoms with corresponding orbital moments for $ACuIn(PO_4)_2$ crystals are plotted in Figure S10. A characteristic feature of this distribution is that the upper valence bands (from -6 to 0 eV) consist almost entirely of p electrons from the oxygen atoms of the PO_4^{3-} anionic groups and a small number of d electrons from the Cu^{2+} ions. The bottom of the CB band of a crystal is generally composed of the s and p-states of indium, and the small existence of the p-states of phosphates.

3.4.2. Calculated optical properties

The investigation of linear optical properties has also been carried out. The linear response of a system to an external electromagnetic field with a small wave vector is evaluated by the complex dielectric function $\varepsilon(\omega) = \varepsilon_{Re}(\omega) + i\varepsilon_{Im}(\omega)$. The imaginary part depends on the frequency and can be calculated using the following equation [53]:

$$\varepsilon_{Im}(\omega) = \frac{2\pi e^2}{\Omega\varepsilon_0} \sum_{k,v,c} |\psi_k^c|\mu.r|\psi_k^v|^2 \delta(E_k^c - E_k^v - h\omega) \quad (2)$$

Where $h\omega$ represents the incident phonon energy, Ω is the volume, and ε_0 is the vacuum dielectric constant. The symbols *v* and c are for the valence and conduction bands, respectively. $\mu.r$ is the momentum operator, while ψ_k^v and ψ_k^c are the VB and CB wave functions, respectively.

The imaginary part of the dielectric function, $\varepsilon_{Im}(\omega)$, can be assimilated to a detail of the real transitions between occupied and unoccupied electronic states. Since the dielectric constant describes a causal response, the real and imaginary parts are linked by a Kramers–Kronig transform:

$$\varepsilon_{Re}(\omega) - 1 = \frac{2}{\pi} P \int_0^{\propto} \frac{\omega' \varepsilon_2(\omega') d\omega'}{\omega'^2 - \omega^2} \text{ (3) and } \varepsilon_{Im}(\omega) = \frac{-2\omega}{\pi} P \int_0^{\propto} \frac{\omega' \varepsilon_1(\omega') d\omega'}{\omega'^2 - \omega^2} \text{ (4)}$$

For this case, P corresponds to the principal value of the integral. This transformation is applied to determine the real part of the dielectric function $\varepsilon_{Re}(\omega)$. The term $\varepsilon_{Re}(\omega)$ tells us about the polarization while $\varepsilon_{Im}(\omega)$ corresponds to the energy loss in a medium and is always positive. The complex dielectric function is also used to find the other optical properties such as conductivity (σ) and absorption coefficient (Abs) [54]:

$$\sigma = \frac{\omega}{2\pi} \varepsilon_{Im}(\omega) \quad (5)$$

$$Abs = \frac{2k\omega}{c} \quad (6)$$

The variation of the wavelength-dependent dielectric function and the corresponding optical properties (σ and Abs) are shown for $ACuIn(PO_4)_2$ crystals in Figure S11. The term $\varepsilon_{Im}(\omega)$ at short photon wavelengths has a value close to 0 for this crystal. Then, the intensity increases in the near-infrared region. This evolution trend is the same for the absorption spectra and also, it matches very well with the above results determined by reflectance spectroscopy. Optical conductivity is the electrical conductivity in the presence of an alternating electric field; the term "optical" covers the entire frequency range and is not limited to the visible light region exclusively. The real part of the optical conductivity represents the in-phase current, which

drives the resistive joule heating, while the imaginary part involves a dephase of π/2 rad of the inductive current.

Here, from the calculated real part of the optical conductivity, we can see that the intensity increases when the incident photon is in the near infrared spectral range for the three kind of crystals, indicating that $ACuIn(PO_4)_2$ is expected to be highly electrically conductive in this optical range.

4. Conclusion

Two orthophosphates single crystals, $KCuIn(PO_4)_2$ and $RbCuIn(PO_4)_2$, have been successfully synthesized by the flux method and their structures have been determined by single crystal X-ray diffraction analysis. In addition, they have also been prepared as powder by means of the solid state reaction method. They are monoclinic and crystallize in the $P2_1/n$ space group. Both crystals are isotopic with $KCuFe(PO_4)_2$. Their structures exhibit a three-dimensional framework formed by Cu_2O_8 dimers linked to PO_4 tetrahedra through an edge and corner, and to InO_6 octahedra via corner creating a zigzag chains parallel to the [110] direction. The projection of the structure in the (101) plane displays hexagonal tunnels evolving in the [001] direction, occupied by the alkali ions. The EDX analysis confirmed the chemical composition of the synthesized compounds. The FTIR and Raman spectroscopies confirmed the appearance of diverse vibration modes corresponding to PO_4 groups. The calculated band structures show that the solid-state compounds of $ACuIn(PO_4)_2$ with (A = K, Rb, Na) are indirect band gap semiconductors with a direct band gap of 2.315, 2.319 and 2.095 eV, respectively. The short UV cut-off edge and the high thermal stabilities show that they are promising optical materials with transparency in the UV.

Acknowledgements

This research article has been possible with the support of the Secretaria d'Universitats i Recerca del Departament d'Empresa i Coneixement de la Generalitat de Catalunya, the European Union (UE), and the European Social Fund (ESF) (2021 FI_B1 00170). Grant PID2019-108543RB-I00 funded by MCIN/AEI/ 10.13039/501100011033.

References

[1] H. Y.-P. Hong, Mater. Res. Bull. 11 (2) (1976) 173–182.

[2] D. J. Fisher, Am. Mineral. 40 (1955) 1100-1109.

[3] W. H. Baur, Phys. Chem. Miner. 2(1) (1977) 3-20.

[4] K. Trad, D. Carlier, L. Croguennec, A. Wattiaux, M. Ben Amara, C. Delmas, Chem. Mater. (2010) 22(19) 5554-5562.

[5] Q. Zheng, H. Yi, X. Li, H. Zhang, J. Energy Chem. 27(6) (2018) 1597-1617.

[6] B. Lang, B. Ziebarth, C. Elsässer, Chem. Mater. 27(14) (2015) 5040-5048.

[7] R. Essehli, I. Belharouak, H. B. Yahia, K. Maher, A. Abouimrane, B. Orayech, Y. K. Sun, Dalton Trans. 44(17) (2015) 7881-7886.

[8] J. Kim, H. Kim, I. Park, Y. U. Park, J. K. Yoo, K. Y. Park, K. Kang, Energy Environ. Sci. 6(3) (2013) 830-834.

[9] C. A. Fisher, V. M. Hart Prieto, M. S. Islam, Chem. Mater. *20*(18) (2008) 5907-5915.

[10] J. J. Carvajal, I. Parreu, R. Solé, X. Solans, F. Diaz, M. Aguilo, Chem. Mater. 17(26) (2005) 6746-6754.

[11] M. E. Hagerman, K. R. Poeppelmeier, Chem. Mater. 7(4) (1995) 602-621.

[12] M. Ono, K. Shimanoe, N. Miura, N. Yamazoe, Solid State Ionics, 136 (2000) 583-588.

[13] A. Badri, I. Alvarez-Serrano, M. Luisa López, M. Ben Amara, Acta Crystallogr. E: Crystallogr. Commun. 76(8) (2020) 1369-1372.

[14] A. Ould Saleck, A. Assani, M. Saadi, C. Mercier, C. Follet, L. El Ammari, Acta Crystallogr. E: Crystallogr. Commun. 74(9) (2018) 1358-1361.

[15] F. Hatert, R. P. Hermann, G. J. Long, A. M. Fransolet, F. Grandjean, Am. Mineral. 88(1) (2003) 211-222.

[16] F. Hatert, D. Antenucci, A. M. Fransolet, M. Liégeois-Duyckaerts, J. Solid State Chem. 163(1) (2002) 194-201.

[17] M.G. Zhizhin, V.A. Morozov, A.P. Bobylev, A.M. Popov, F.M. Spiridonov, L.N. Komissarova, B.I. Lazoryak, J. Solid State Chem. 149(1) (2000) 99-106.

[18] A. Arakcheeva, G. Chapuis, V. Petříček, M. Dušek, A. Schönleber, Acta Crystallogr. B: Struct. Sci. Cryst. Eng. Mater 59(1) (2003) 17-27.

[19] J. K. Nimmo, Acta. Crystallogr. B. Struct. Sci. Cryst. 37(2) (1981) 431-433.

[20] M. G. Zhizhin,; A. A. Filaretov,; A. V. Olenev,; V. V. Chernyshev, F. M. Spiridonov, L. N. Komissarova, Crystallogr. Rep. 47(5) (2002) 773-782.

[21] E. Benhsina, J. Khmiyas, S. Ouaatta, A. Assani, M. Saadi, L. El Ammari, Acta Crystallogr. E: Crystallogr. Commun. 76(3) (2020). 366-369.

[22] Stoe, Cie. "X-AREA, version 1.30, program for the acquisition and analysis of data." Stoe & Cie GmbH, Darmatadt, Germany (2005).

[23] Stoe, Cie, and Version X-RED. "1.28 b: Program for data reduction and absorption correction." Stoe & Cie GmbH, Darmstadt, Germany (2005).

[24] Stoe, Cie. "X-SHAPE, version 2.05, program for crystal optimization for numerical absorption correction." Stoe & Cie GmbH, Darmatadt, Germany (2004).

[25] A. Altomare, G. Cascarano, C. Giacovazzo, A. Guagliardi, J. Appl. Crystallogr. 26 (1993) 343-350.

[26] G.M. Sheldrick, SHELXT: integrating space group determination and structure solution, Acta Crystallogr. Sect. Found Adv. 70 (2014) C1437.

[27] S.J. Clark, M.D. Segall, C.J. Pickard, P.J. Hasnip, M.I.J. Probert, K. Refson, M.C. Payne, Zeitschrift Fur Krist. 220 (2005) 567–570.

[28] A. Faucher, V. V. Terskikh, R.E. Wasylishen, Solid State Nucl. Magn. Reson. 61–62 (2014) 54–61.

[29] M. Zhou, X. Jiang, C. Li, Z. Lin, J. Yao, Y. Wu, Zeitschrift Für Anorg. Und Allg. Chemie. 641 (2015) 2321–2325.

[30] A.M. Rappe, K.M. Rabe, E. Kaxiras, J.D. Joannopoulos, Phys. Rev. B. 41 (1990) 1227–1230.

[31] M. Nespolo, B. Guillot, J. Appl. Cryst. 49 (2016) 317–321.

[32] K. H. Lii, J. Ye, J. Solid State Chem. 131(1) (1997) 131-137.

[33] H. A. Jahn, E. Teller, Proc. R. Soc. London, Ser. A. 161 (1937) 220-235.

[34] X. Assfeld, F. Volatron, L'actualité chim. 350 (2011) 26-34.

[35] W. H. Bauer, Acta Crystallogr. 30(1974) 1195.

[36] G. Donnay, R. Allman Am. Mineral. 55 (1970) 1003.

[37] O. Yakubovich, G. Kiriukhina, L. Shvanskaya, A. Volkov, O. Dimitrova, Acta Crystallogr., Sect. B: Struct. Sci., Cryst. Eng. Mater.76(3) (2020) 483-491.

[38] O. V. Yakubovich, G. V. Kiriukhina, O. V. Dimitrova, E. A. Zvereva, L. V. Shvanskaya, O. S. Volkova, A. N. Vasiliev, Dalton Trans. 45(6) (2016) 2598-2604.

[39] X. H. Chen, R. Z. Guo, Y. X. Huang, Y., Pan, J. X. Mi, Dalton Trans. 50(22) (2021) 7835-7842.
[40] A. Badri, M. Hidouri, M. L. Lopez, C. Pico, A.Wattiaux, M. Ben. Amara, J. Solid State Chem. 184(4) (2011) 937-944.
[41] A. Badri, M. Hidouri, M. Ben. Amara, Acta Crystallogr. E69(8) (2013) i52-i52.
[42] A. Akhrouf, Y. Laajali, M. Haddad, E.K. Hlil, S. Krimi, J. Mol. Struct. 1258 (2022) 132640.
[43] J. Rodríguez-Carvajal, Physica B 192 (1993) 55.
[44] N.M.A. Hadia, H.A. Mohamed, J. Alloys Compd. 547 (2013) 63-67.
[45] B. PANalytical, X'Pert HighScore Plus, X'Pert HighScore Plus, Lelyweg, Almelo, the Netherlands 2 (2002).
[46] S.D. Ross, Inorganic Infrared and Raman Spectra, McGraw-Hill Book Company, (1972) London.
[47] C. J. Antony, A. Aatiq, C. Y. Panicker, M. J. Bushiri, H. T. Varghese, T. K. Manojkumar,. Spectrochim. Acta - Part A Mol. Biomol.78 (2011) 415-419.
[48] M.J. Bushiri, R.S. Jayasree, M. Fakhfakh, V.U. Nayar, Mater. Chem. Phys. 73(2-3) (2002). 179-185.
[49] X. Hu, L. Liu, S. Zhai, Spectrochim. Acta A Mol. Biomol. Spectrosc. 245 (2021) 118906.
[50] T. Jenkins, J. A. Alarco, I. D. Mackinnon, ACS omega, 6(3) (2021) 1917-1929.
[51] M. Jiao, C. Yang, M. Liu, Q. Xu, Y. Yu, H. You, Opt. Mater. Express. 7(7) (2017) 2660-2671.
[52] M. Dalal, J. Dalal, S. Chahar, H. Dahiya, S. Devi, P. Dhankhar, S. Kumar, V.B. Taxak, D. Kumar, S.P. Khatkar, J. Alloys Compd. 805 (2019) 84–96.
[53] D. Zhao, H. Zhang, Z. Xie, W.L. Zhang, S.L. Yang, W.D. Cheng, J. Chem. Soc. Dalt. Trans. 2 (2009) 5310–5318.
[54] J. Jiao, W. Jin, M. Zhang, Z. Yang, S. Pan, J. Mol. Struct. 1226 (12934) (2021) 129349.

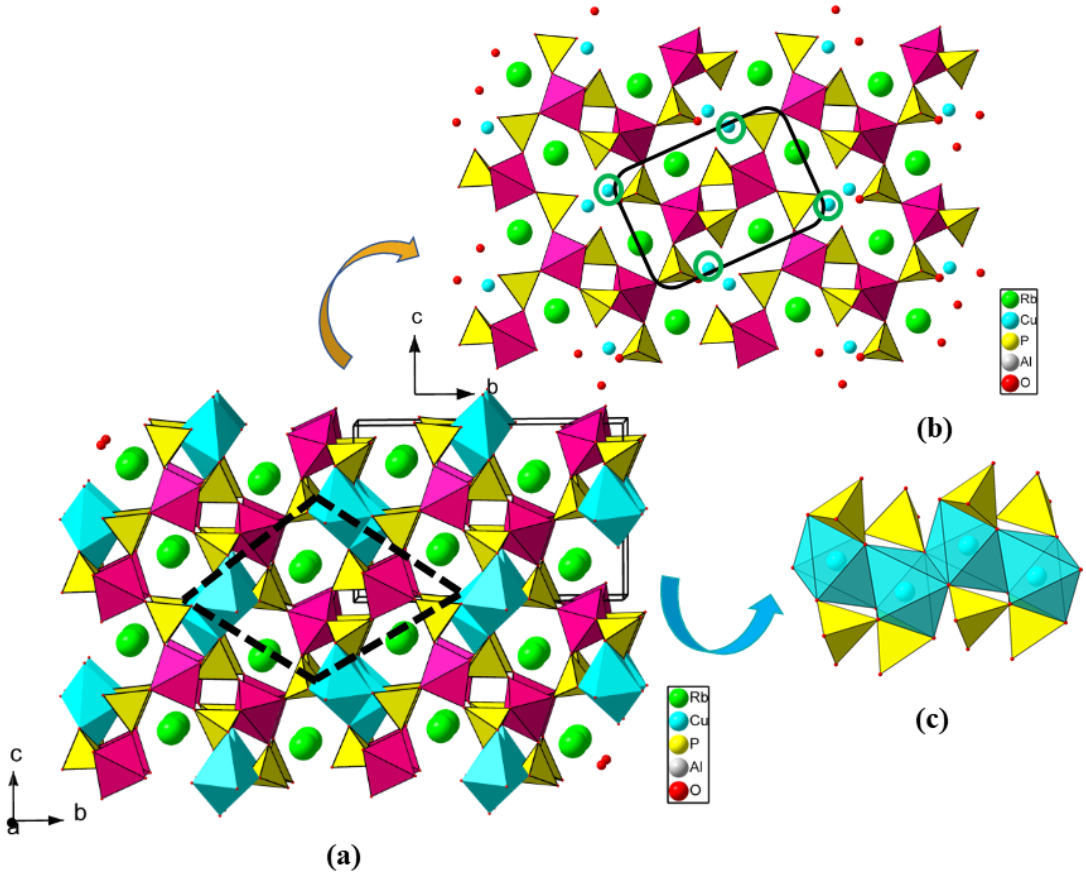


Figure 1.

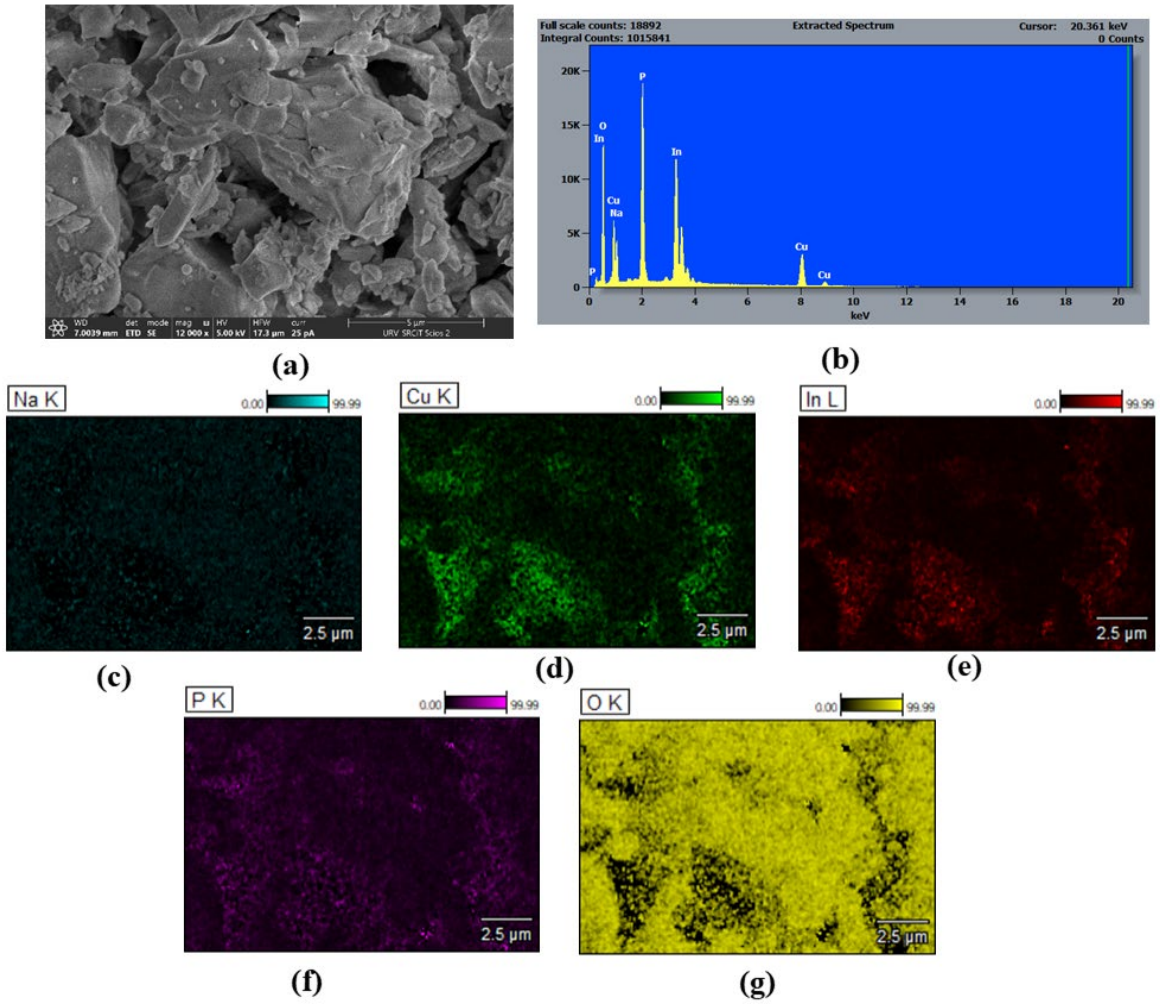


Figure 2.

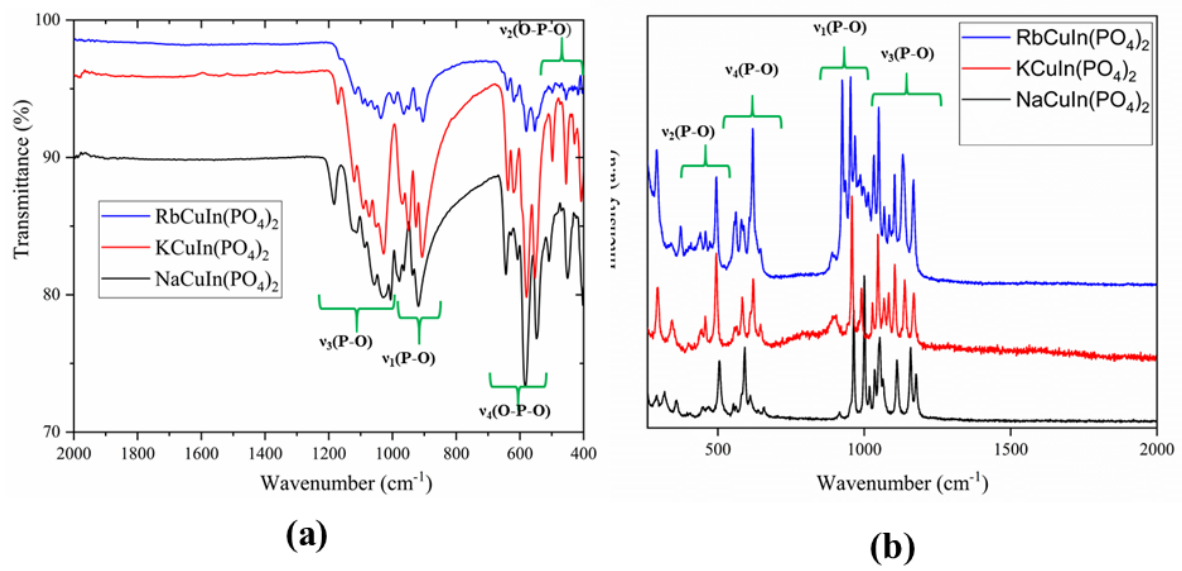


Figure 3.

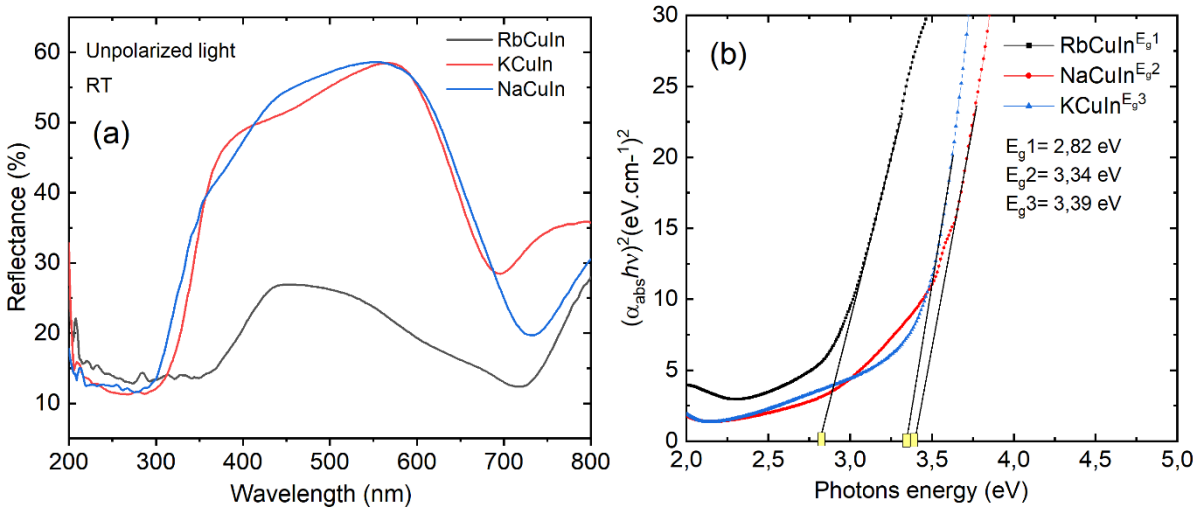

Unpolarized light
RT
(a)
RbCuIn
KCuIn
NaCuIn
Reflectance (%)
Wavelength (nm)
(b)
RbCuIn^{E_g1}
NaCuIn^{E_g2}
KCuIn^{E_g3}
E_g1= 2,82 eV
E_g2= 3,34 eV
E_g3= 3,39 eV
$(\alpha_{abs}h\nu)^2$(eV.cm^{-1})^2
Photons energy (eV)

Figure 4.

Table 1: Crystallographic data and structure refinement for $ACuIn(PO_4)_2$ (A=K, Rb).

Crystal data		
Chemical formula	$KCuIn(PO_4)_2$	$RbCuIn(PO_4)_2$
Crystal system	Monoclinic	Monoclinic
Space group	$P2_1/n$	$P2_1/n$
a (Å)	8.1970(8)	8.2942(7)
b (Å)	10.1716(8)	10.1497(8)
c (Å)	9.740(9)	9.3102(8)
β(°)	115.702(7)	115.682(7)
Z	4	4
Data collection		
Crystal size (mm)	0.28×0.32×0.42	0.34×0.56×0.67
Diffractometer	STOE IPDS-II	STOE IPDS-II
Radiation	λ (Mo K_α) = 0.7107 Å	λ (Mo K_α) = 0.7107 Å
Monochromator	Graphite	Graphite
μ(mm^{-1})	7,510	13.586
Scan type	ω/2θ	ω/2θ
Scan speed	Variable	Variable
$2\theta_{max}$ (°)	3.43-37.55	4.02-38.28
Number of unique reflections; R_{int}	1343; R_{int} = 0.019	3877; R_{int} = 0.086
Number of observed reflections [I>2σ(I)]	1328	3305
Indices	-10 ≤ h ≤ 9 ; -12≤ k≤12; -11 ≤ l ≤ 11	-14 ≤ h ≤ 14 ; -17≤ k≤17; -15 ≤ l ≤ 16
F (000)	764	836
Structural refinement		
Intensity corrections	Lorentz-polarization	Lorentz-polarization
Absorption correction ($T_{min,\ max}$)	Integration (0.3264; 0.4491)	Integration (0.0138; 0.1063)
Structure solution	Direct Method	Direct Method
Reliability factors	R_1= 0.023; wR_2= 0.052; S = 1.364	R_1= 0.059; wR_2= 0.0145; S = 1.364
Number of parameters	119	119
$(\Delta\rho)_{max,\ min}$/e. $Å^{-3}$	1.094; -0.459	3.667; -2.188

Table 2: Structural data of the compounds with formula $ACuM^{III}(PO_4)_2$ with (A= Na^+, K^+ and Rb^+) and (M^{III}= Al^{3+}, Ga^{3+}, In^{3+}, Cr^{3+} et Fe^{3+}).

Formula	Space group	Cell parameters			M^{2+}/O	M^{3+}/O	
		a(Å)	b(Å) β(°)	c(Å)			
$KCuAl(PO_4)_2$	$P2_1/c$	5.0270(8)	14.047(2) 102.29(1)	9.263(1)	**[6]**	**[5]**	[37]
$RbCuAl(PO_4)_2$		5.0723(8)	14.070(2) 100.41(1)	9.352(1)			[38]
$KCuGa(PO_4)_2$		4.977(3)	14.025(8) 101.906(8)	9.376(5)			[39]
$KCuFe(PO_4)_2$	$P2_1/n$	7.958(3)	9.931(2) 115.59(3)	9.039(2)	**[5]**	**[6]**	[40]
$RbCuFe(PO_4)_2$		8.054(1)	9.906(3) 115.47(1)	9.140(1)			[41]
$KCuCr(PO_4)_2$		7.861(2)	9.828(2) 115.2(1)	9.002(2)			[42]
$NaCuIn(PO_4)_2$		8.237(3)	10.121(2) 114.508(2)	8.802(3)			[21]
$KCuIn(PO_4)_2$		8.1970(8)	10.1716(8) 115.702(7)	9.1740(9)			This work
$RbCuIn(PO_4)_2$		8.2942(7)	10.1497(8) 115.682(7)	9.3102(8)			This work